Research Square

Preprints are preliminary reports that have not undergone peer review.
They should not be considered conclusive, used to inform clinical practice,
or referenced by the media as validated information.

Suppression of propellant sloshing in a spacecraft tank: a two-sided upwind implicit–explicit difference scheme for a Saint-Venant model with nonlocal feedback and its exponential stability in the sense of Lyapunov

S.U. Dadabaev

sdusardor1986@gmail.com

Kokand UniversityAndijan Branch

R. D. Aloev

National University of Uzbekistan named after Mirzo Ulugbek

Article

Keywords: propellant sloshing, Saint-Venant equations, nonlocal feedback, dissipative boundary conditions, discrete Lyapunov function, implicit upwind scheme, exponential stability

Posted Date: November 20th, 2026

DOI: https://doi.org/10.21203/rs.3.rs-11783071/v1

License: This work is licensed under a Creative Commons Attribution 4.0 International License.
Read Full License

Additional Declarations: No competing interests reported.

Suppression of propellant sloshing in a spacecraft tank: a two-sided upwind implicit–explicit difference scheme for a Saint-Venant model with nonlocal feedback and its exponential stability in the sense of Lyapunov

S. U. Dadabayev [1]; R. D. Aloev [2];

[1] Kokand UniversityAndijan Branch, Andijan, Uzbekistan

[2] National University of Uzbekistan named after Mirzo Ulugbek, Tashkent, Uzbekistan. E-mail: sdusardor@mail.ru

Word Count: 4065 words (main body) with 9 figures and 6 tables

Article submitted to: Journal of Mathematical Fluid Mechanics

Version: 1

Corresponding author: S. U. Dadabayev, Andijan Branch of Kokand University, Andijan, Uzbekistan.

E-mail: sdusardor1986@gmail.com

Acknowledgments

The research was carried out at the authors' own expense.

Abstract

Sloshing of liquid propellant, which accounts for a large share of the mass of launch-vehicle stages and spacecraft, exerts a time-varying force on the vehicle and degrades attitude-control and manoeuvre accuracy. In this paper the longitudinal sloshing of propellant settled at the tank bottom by engine thrust is modelled by the Saint-Venant (shallow-water) equations written in coordinates attached to the tank. One end of the tank is a rigid wall, the other a damped elastic diaphragm; for the diaphragm, conservation of volume introduces a *nonlocal* term (the integral of the free-surface elevation) into the boundary condition. The acceleration of the vehicle is chosen proportional to the total momentum of the liquid relative to the tank, $a(t) = kP(t)$, $P = \int_0^1 v\ \mathrm{d}x$; this enters the equations as a second nonlocal term, a spatially uniform source. The linearized problem is written in Riemann invariants, and a new *two-sided upwind implicit–explicit scheme* is constructed for it: the two characteristic families are computed by implicit sweeps in opposite directions, the two boundaries are coupled at the new time level by a closed-form formula, and the nonlocal source and the nonlocal boundary term are treated explicitly. For a classical discrete Lyapunov function with exponential weights adapted to the direction of wave propagation, the inequality $V^{n+1} \le q_* V^n$, $q_* < 1$, is proved under conditions depending explicitly on the grid parameters; these conditions do not require the Courant–Friedrichs–Lewy (CFL) condition. In the passive case ($k = 0$) the estimate coincides with the exact spectral decay rate. A stability theorem is also proved for a second scheme, the predictor–corrector B-variant, which evaluates the nonlocal terms at the half time level; it halves the nonlocal lag error and, under strong feedback with large time steps, remains stable in the region where the A-variant is unstable. As consequences, estimates are obtained for the cumulative dissipation of momentum and for the total velocity change Δv of the vehicle. It is shown that with rigid walls there is no exponential decay for any k, and that the system is unstable for $k < 0$. Spectral analysis shows that the feedback raises the damping ratio of the fundamental sloshing mode from 1.7% to 27%, and numerical experiments show an 18–50-fold reduction of the sloshing force. For deep (full) tanks the model is extended by an *equivalent depth* consistent with finite-depth dispersion: it reproduces the frequency and the sloshing mass of the fundamental mode exactly as given by potential theory, while the dimensionless equations, the scheme and the theorem remain unchanged. The results are applied to the 623 L P/N 80451-1 hydrazine tank used on the WorldView-4 (GeoEye-2) spacecraft.

Key words: propellant sloshing; Saint-Venant equations; nonlocal feedback; dissipative boundary conditions; discrete Lyapunov function; implicit upwind scheme; exponential stability.

MSC 2020: 65M06, 65M12, 35L50, 93D15, 76B15.

Abbreviations: 1D: one-dimensional; CFD: computational fluid dynamics; CFL: Courant–Friedrichs–Lewy; IMEX: implicit–explicit; PDE: partial differential equation.

1. INTRODUCTION

1.1. Motivation

In liquid-propellant launch-vehicle stages and spacecraft, propellant constitutes a substantial fraction of the total mass. When the vehicle accelerates, rotates, or when the engine is started or shut down, the liquid in the tank sloshes and exerts a time-varying force and moment on the structure. If the sloshing frequency is close to the frequencies of the control system, sloshing may resonate with the attitude-control system, lengthen the settling time after a manoeuvre and spoil precise pointing; these problems have been studied extensively in space engineering [1-3]. Passive devices (baffles, diaphragms) usually provide only a few percent of damping of the fundamental mode, so active suppression, i.e. suppression by means of control, is of practical importance.

1.2. Literature Review

The Saint-Venant model of a liquid moving together with a tank and the associated motion-planning problem were formulated by Dubois, Petit and Rouchon [4]. Petit and Rouchon [5] showed that the linearized system for a flat-bottomed tank is not controllable; Coron [6] proved local controllability of the nonlinear system around equilibrium by the return method, and in [7] the stabilization of the system linearized around a constant acceleration was solved. The theory of stabilization of one-dimensional (1D) hyperbolic systems by dissipative boundary conditions was developed in [8-10], its discrete counterparts in [11, 12], and the stability of numerical solutions of systems with nonlocal characteristic velocities in the works of R. D. Aloev and co-authors [13-15]. However, Lyapunov stability of a *discrete* model of the tank problem, especially when nonlocal feedback and a nonlocal boundary condition act simultaneously, remains open.

1.3. Contribution of the Paper

1. For a tank with a damped elastic diaphragm, a linearized model is derived in Riemann invariants with a *nonlocal boundary condition* resulting from volume conservation and a *nonlocal source* resulting from momentum feedback on the vehicle acceleration (Lemma 1).
2. A new two-sided upwind implicit–explicit (IMEX) scheme is constructed; the boundary-closure formula and its unique solvability are proved (Lemma 3).
3. The main stability theorem is proved for a classical discrete Lyapunov function with exponential weights (Theorem 1); it does not require the Courant–Friedrichs–Lewy (CFL)

condition and is sharp in the passive case. As corollaries, estimates for the dissipation of momentum and for Δv are obtained.

4. A predictor–corrector B-variant for the nonlocal terms is constructed, and a discrete momentum balance (Lemma 7) and its stability theorem (Theorem 2) are proved; the accuracy of the A- and B-variants and their stability for large time steps are compared.
5. It is shown that stabilization without passive damping is impossible (Proposition 1) and that the system is unstable for $k < 0$ (Proposition 2); a formula for choosing k to damp the fundamental mode is given (Proposition 4).
6. The model is extended to deep liquid by means of an equivalent depth, and it is proved that it gives the fundamental-mode frequency and sloshing mass exactly (Proposition 3); the results are applied to a real tank (P/N 80451-1, WorldView-4).
7. The numerical experiments analyse linear and nonlinear models, stable and unstable regimes, numerical instability associated with the CFL condition, and the influence of numerical dissipation.

2. PROBLEM FORMULATION

2.1. Liquid in a Moving Tank

A rectangular tank of length L moves together with the vehicle along the x-axis with acceleration $a(t)$. The effective acceleration g_e produced by the engine thrust settles the propellant at the tank bottom (settled propellant); in tank coordinates the liquid depth $H(t,x)$ and the relative velocity $V(t,x)$ satisfy the Saint-Venant equations [4, 5]:

$$H_t + (HV)_x = 0, \qquad V_t + (g_e H + 1/2\, V^2)_x = -a(t). \qquad (1)$$

We nondimensionalize x by L, H by the equilibrium depth H_0, V by $c = \sqrt{g_e H_0}$, t by L/c, and a by c^2/L. Linearizing for small sloshing amplitudes with $H = 1 + h$, $V = v$, we obtain

$$h_t + v_x = 0, \qquad v_t + h_x = -a(t), \qquad x \in (0,1). \qquad (2)$$

For the Riemann invariants $R = v + h$, $S = v - h$,

$$R_t + R_x = -a(t), \qquad S_t - S_x = -a(t), \qquad v = R + S/2\,, \quad h = R - S/2\,. \qquad (3)$$

In the linear approximation, the horizontal force exerted by the liquid on the tank walls (dimensionless, in units of $\rho g_e H_0^2$) equals

$$F_s(t) = h(t,1) - h(t,0); \qquad (4)$$

it is precisely this *sloshing force* that acts on the vehicle dynamics.

2.2. Boundary Conditions and Nonlocality

The wall at $x = 0$ is rigid: $v(t,0) = 0$, i.e. $R(t,0) = -S(t,0)$. The wall at $x = 1$ is a damped elastic diaphragm (diaphragm tank) with displacement $w(t)$, velocity $\dot{w} = v(t,1)$, and pressure balance

$$h(t,1) = \zeta_d\, v(t,1) + \kappa\, w(t), \qquad \zeta_d > 0,\ \kappa \geq 0. \qquad (5)$$

Lemma 1. *If the liquid volume is conserved, i.e.* $\int_0^1 h\,(0,x)\,\mathrm{d}x + w(0) = 0$, *then* $w(t) = -\mathcal{H}(t)$ *for all* $t \geq 0$, *where* $\mathcal{H}(t) := \int_0^1 h\,(t,x)\,\mathrm{d}x$, *and condition (5) takes, in Riemann invariants, the form*

$S(t,1) = -r\,R(t,1) + \eta\,\mathcal{H}(t), \qquad r = \frac{\zeta_d - 1}{\zeta_d + 1} \in (-1,1), \quad \eta = \frac{2\kappa}{1+\zeta_d} \geq 0. \qquad (6)$ *Since* $\mathcal{H} = \frac{1}{2}\int_0^1 (R - S)\ \mathrm{d}x$, *(6) is a nonlocal boundary condition.*

Proof. From (2), $\frac{d}{dt}\int_0^1 h\ \mathrm{d}x = -\big(v(t,1) - v(t,0)\big) = -\dot{w}$; hence $\int_0^1 h\ \mathrm{d}x + w$ is conserved. Substituting $h = (R - S)/2$, $v = (R + S)/2$, $w = -\mathcal{H}$ into (5), we get $R - S = \zeta_d(R + S) - 2\kappa\mathcal{H}$, i.e. $S(1 + \zeta_d) = -(\zeta_d - 1)R + 2\kappa\mathcal{H}$. □

As $\zeta_d \to \infty$ (rigid wall), $r \to 1$ and $\eta \to 0$; for $\zeta_d = 1$, $r = 0$ (perfectly absorbing wall). The quantity r is the reflection coefficient of the wall.

2.3. Momentum Feedback

The transverse acceleration of the vehicle (along the tank axis) is prescribed by the control system as

$$a(t) = k\,P(t), \qquad P(t) = \int_0^1 v\,(t,x)\,\mathrm{d}x = \frac{1}{2}\int_0^1 (R + S)\ \mathrm{d}x, \qquad k \geq 0: \qquad (7)$$

the tank is accelerated in the direction of the relative motion of the liquid, and the relative momentum is "absorbed". Since P is an integral over the whole tank, the source in (3) is *nonlocal*: the liquid at every point experiences the same inertial force, which depends on the state of the whole liquid. The total velocity change of the vehicle, $\Delta v(t) = \int_0^t a\ \mathrm{d}s$, is the "velocity budget" spent on control.

Lemma 2 (Energy identity). *Let* $\eta = 0$. *Then for smooth solutions the energy* $E(t) = \frac{1}{2}\int_0^1 (h^2 + v^2)\ \mathrm{d}x = \frac{1}{4}\int_0^1 (R^2 + S^2)\ \mathrm{d}x$ *satisfies* $\frac{dE}{dt} = -\frac{1-r^2}{4}R(t,1)^2 - k\,P(t)^2$. $\qquad (8)$

Proof. Multiplying (3) by $R/2$ and $S/2$ and integrating, we obtain $\frac{dE}{dt} = \frac{1}{4}(R(0)^2 - R(1)^2 + S(1)^2 - S(0)^2) - \frac{a}{2}\int_0^1 (R+S)\ \mathrm{d}x$. Identity (8) follows from $R(0)^2 = S(0)^2$, $S(1)^2 = r^2 R(1)^2$, $\frac{1}{2}\int (R+S) = P$ and $a = kP$. □

Proposition 1 (Stabilization without passive damping is impossible). *Let $r = 1$, $\eta = 0$ (both walls rigid). Then for every k problem (2), (7) has the solution $h = \varepsilon\cos(2\pi x)\cos(2\pi t)$, $v = \varepsilon\sin(2\pi x)\sin(2\pi t)$; its energy is constant and $P \equiv 0$. Hence the equilibrium is not asymptotically stable.*

Proof. Direct verification: $h_t + v_x = 0$, $v_t + h_x = 0$, $v(t,0) = v(t,1) = 0$, $\int_0^1 \sin(2\pi x)\,\mathrm{d}x = 0$, i.e. $a \equiv 0$; $E = \varepsilon^2/4$. □

This result is the stabilization counterpart of the lack of controllability established in [5]: the even modes give $P = 0$ and $F_s = 0$, so the motion of the tank cannot affect them; they are damped only by passive dissipation ($r < 1$).

Proposition 2 (Energy growth for $k < 0$). *If $\eta = 0$, $r = 1$, $k < 0$, then (8) gives $\dot{E} = |k|P^2 \geq 0$; the energy grows for every solution with $P \not\equiv 0$, and the equilibrium is not asymptotically stable.*

2.4. Depth-Corrected Equivalent Model

The Saint-Venant model takes the wave speed to be $c = \sqrt{g_e H_0}$, which is valid for $H_0/L \ll 1$. By linear potential theory, the natural frequency of the nth mode in a rectangular tank of length L with liquid depth H_0 is [1, 3]

$$\omega_n^2 = \frac{n\pi g_e}{L}\tanh\frac{n\pi H_0}{L}. \qquad (9)$$

We introduce the *equivalent depth* and the *equivalent wave speed*

$$H_e = \frac{L}{\pi}\tanh\frac{\pi H_0}{L}, \qquad c_e = \sqrt{g_e H_e}, \qquad (10)$$

and replace H_0 by H_e in the linearized model: $h_t + H_e v_x = 0$, $v_t + g_e h_x = -a$. Nondimensionalization is performed with c_e and L/c_e; as a result, (2)–(3), the boundary conditions and (7) remain *exactly the same*. Consequently, the scheme of Section 3, Theorem 1 and its corollaries remain fully valid for the equivalent model; only the dimensional units of time, velocity and force are computed via c_e.

Proposition 3 (Calibration on the fundamental mode). *For a tank of width b, the equivalent model*

1. *gives the fundamental-mode frequency exactly: $\omega_1 = \pi c_e/L$ equals ω_1 in (9);*

2. *gives the sloshing mass of the fundamental mode exactly:* $m_1 = \frac{8}{\pi^2}\rho H_e L b$, *i.e.* $\frac{m_1}{m} = \frac{8L}{\pi^3 H_0}\tanh\frac{\pi H_0}{L}$, $\quad m = \rho H_0 L b, \quad (11)$ *which coincides with the value in the classical equivalent mechanical model [1, 3];*

3. *reduces to the shallow-water model as* $H_0/L \to 0$, *since then* $H_e \to H_0$;

4. *gives* $\omega_n = n\omega_1$ *for the higher modes, whereas the exact value is* $\omega_n = \omega_1 \left(\frac{n\tanh(n\pi H_0/L)}{\tanh(\pi H_0/L)}\right)^{1/2}$; *the relative error in the second-mode frequency is* 8% *for* $H_0/L = 0.14$ *and* 40% *for* $H_0/L = 0.79$.

Proof. (a) $\omega_1^2 = \pi^2 g_e H_e/L^2 = (\pi g_e/L)\tanh(\pi H_0/L)$. (b) Under horizontal excitation the modal mass of the nth mode is $m_n = \rho H_e b \left(\int_0^L \phi_n \, \mathrm{d}x\right)^2 / \int_0^L \phi_n^2 \, \mathrm{d}x$, where the velocity mode shape is $\phi_1 = \sin(\pi x/L)$: $\left(\int_0^L \phi_1\right)^2 / \int_0^L \phi_1^2 = (2L/\pi)^2/(L/2) = 8L/\pi^2$; substituting H_e from (10) yields (11). (c) $\tanh z \sim z$. (d) In the shallow-water model the frequencies are $n\pi c_e/L$; the exact value follows from (9). □

Since the feedback, the scheme and the theorem are aimed at the fundamental mode (which provides the main part of the sloshing force, Proposition 4), the equivalent model describes exactly the mode that matters; the frequencies of the higher modes are reliable only at low fill levels.

3. TWO-SIDED UPWIND IMPLICIT–EXPLICIT SCHEME

Let $x_j = jh$, $h = 1/J$, $t_n = n\tau$, $\sigma = \tau/h$. The unknowns for R are R_j^n, $j = 1, \dots, J$ (R_0^n is the inflow boundary value), and those for S are S_j^n, $j = 0, \dots, J-1$ (S_J^n is the inflow boundary value). The nonlocal quantities are computed by the rectangle rule:

$$P^n = \frac{h}{2}\left(\sum_{j=1}^{J} R_j^n + \sum_{j=0}^{J-1} S_j^n\right), \qquad \mathcal{H}^n = \frac{h}{2}\left(\sum_{j=1}^{J} R_j^n - \sum_{j=0}^{J-1} S_j^n\right), \qquad a^n = kP^n. \qquad (12)$$

Scheme:

$$(1+\sigma)R_j^{n+1} = R_j^n + \sigma R_{j-1}^{n+1} - \tau a^n, \qquad j = 1, \dots, J, \qquad (13)$$

$$(1+\sigma)S_j^{n+1} = S_j^n + \sigma S_{j+1}^{n+1} - \tau a^n, \qquad j = 0, \dots, J-1, \qquad (14)$$

$$R_0^{n+1} = -S_0^{n+1}, \qquad S_J^{n+1} = -r\,R_J^{n+1} + \eta\,\mathcal{H}^n. \qquad (15)$$

Transport is implicit and upwind, while the nonlocal source a^n and the nonlocal boundary term $\eta\mathcal{H}^n$ are explicit; the order of accuracy is $O(\tau + h)$. R is computed by a left-to-right sweep and S by a right-to-left sweep; the two families are coupled through (15).

Lemma 3 (Boundary closure). *Let* $b = \big(\sigma/(1+\sigma)\big)^J \in (0,1)$, $A_0 = 0$, $A_j = \big(R_j^n - \tau a^n + \sigma A_{j-1}\big)/(1+\sigma)$, $C_J = 0$, $C_j = \big(S_j^n - \tau a^n + \sigma C_{j+1}\big)/(1+\sigma)$. *Then for* $|r| < 1$ *system (13)–(15) has a unique solution:* $R_0^{n+1} = \frac{-C_0 + r\,b\,A_J - b\,\eta\,\mathcal{H}^n}{1 - r\,b^2}$, $R_j^{n+1} = A_j + (\sigma/1+\sigma)^j R_0^{n+1}$, $S_J^{n+1} = -rR_J^{n+1} + \eta\mathcal{H}^n$, (16) $S_j^{n+1} = C_j + \big(\sigma/(1+\sigma)\big)^{J-j} S_J^{n+1}$. *The cost of one step is* $O(J)$.

Proof. By induction, $R_j^{n+1} = A_J + bR_0^{n+1}$ and $S_0^{n+1} = C_0 + bS_J^{n+1}$. Substituting these into (15) gives $R_0 = -C_0 - b\big(-r\big(A_J + bR_0\big) + \eta\mathcal{H}^n\big)$, whence $(1 - rb^2)R_0 = -C_0 + rbA_J - b\eta\mathcal{H}^n$; note that $|rb^2| < 1$. □

For comparison, the **explicit scheme** is $R_j^{n+1} = (1-\sigma)R_j^n + \sigma R_{j-1}^n - \tau a^n$, $S_j^{n+1} = (1-\sigma)S_j^n + \sigma S_{j+1}^n - \tau a^n$, with the boundary values taken at the new time level.

3.1. B-Variant: Predictor–Corrector for the Nonlocal Terms

From now on the scheme constructed above is called the *A-variant*: in it the nonlocal quantities P^n, $\mathcal{H}^n$ are lagged by one time level. The second scheme, the *B-variant*, built on the implicit–explicit upwind technique for systems with nonlocal velocities [16], evaluates the nonlocal quantities at the half time level. For the sloshing problem it reads as follows:

1. *Predictor*: solve (13)–(15) with $a^n = kP^n$, $\mathcal{H}^n$ to obtain $\big(\tilde{R}, \tilde{S}\big)$, and compute $\tilde{P}^{n+1}$, $\tilde{\mathcal{H}}^{n+1}$ by (12);
2. *Corrector*: with $P^{n+1/2} = \frac{1}{2}\big(P^n + \tilde{P}^{n+1}\big)$, $\mathcal{H}^{n+1/2} = \frac{1}{2}\big(\mathcal{H}^n + \tilde{\mathcal{H}}^{n+1}\big)$, $a^{n+1/2} = kP^{n+1/2}$, solve (13)–(15) *again* from time level n:

$$(1+\sigma)R_j^{n+1} = R_j^n + \sigma R_{j-1}^{n+1} - \tau a^{n+1/2}, \qquad (1+\sigma)S_j^{n+1} = S_j^n + \sigma S_{j+1}^{n+1} - \tau a^{n+1/2},$$
$$R_0^{n+1} = -S_0^{n+1}, \qquad S_J^{n+1} = -rR_J^{n+1} + \eta\,\mathcal{H}^{n+1/2}. \qquad (17)$$

Both stages are solved by the closed-form formula of Lemma 3 (with $a^{n+1/2}$, $\mathcal{H}^{n+1/2}$ in place of a^n, $\mathcal{H}^n$); the cost of one step is $O(J)$, twice that of the A-variant. The nonlocal terms remain explicit: no global (fully implicit) coupled system is solved.

4. DISCRETE LYAPUNOV FUNCTION AND THE MAIN THEOREM

Definition 1. For $\mu > 0$, $q \geq p > 0$, the discrete Lyapunov function is

$$V^n = h\sum_{j=1}^{J} p\; e^{-\mu x_j}\big(R_j^n\big)^2 + h\sum_{j=0}^{J-1} q\; e^{\mu x_j}\big(S_j^n\big)^2. \qquad (18)$$

For each family the weight is largest at its inflow boundary and decreases in the direction of wave propagation; this is the grid analogue of the classical function of [8, 9]. For $\| u^n \|^2 = h\sum_{j=1}^{J}\big(R_j^n\big)^2 + h\sum_{j=0}^{J-1}\big(S_j^n\big)^2$,

$$p\, e^{-\mu} \| u^n \|^2 \le V^n \le q\, e^{\mu(1-h)} \| u^n \|^2. \qquad (19)$$

Grid constants:

$$\nu_h = \frac{1-e^{-\mu h}}{h}, \qquad M_h = h\sum_{j=1}^{J} p\; e^{-\mu x_j} + h\sum_{j=0}^{J-1} q\; e^{\mu x_j}, \qquad Z_h = h\sum_{j=1}^{J}\frac{e^{\mu x_j}}{p} + h\sum_{j=0}^{J-1}\frac{e^{-\mu x_j}}{q},$$

$$\Gamma_h = h\sum_{j=1}^{J} p\;(1-e^{-\mu x_j})^2 e^{\mu x_j} + h\sum_{j=0}^{J-1}\frac{(q\,e^{\mu x_j}-p)^2}{q\,e^{\mu x_j}}, \qquad \vartheta_h = \frac{q\,e^{\mu(1-h)}\eta^2 Z_h}{4(1-(q/p)r^2e^{2\mu})}. \qquad (20)$$

Lemma 4 (Energy identity for the implicit upwind operator). *Let $\sigma > 0$, $w_j = e^{-\mu x_j}$, and $(1+\sigma)u_j = f_j + \sigma u_{j-1}$, $j = 1, \dots, J$. Then $h\sum_{j=1}^{J} w_j f_j^2 = \big(1+\sigma(1-e^{-\mu h})\big)h\sum_{j=1}^{J} w_j u_j^2 + \sigma h e^{-\mu h}\big(e^{-\mu}u_J^2 - u_0^2\big) + \sigma(1+\sigma)h\sum_{j=1}^{J} w_j \big(u_j - u_{j-1}\big)^2$.*

Proof. From $f_j = u_j + \sigma\big(u_j - u_{j-1}\big)$ and $2u_j\big(u_j - u_{j-1}\big) = u_j^2 - u_{j-1}^2 + \big(u_j - u_{j-1}\big)^2$ we get $f_j^2 = u_j^2 + \sigma\big(u_j^2 - u_{j-1}^2\big) + \sigma(1+\sigma)\big(u_j - u_{j-1}\big)^2$. We multiply by hw_j, sum, and apply Abel summation by parts: $\sum_{j=1}^{J} w_j\big(u_j^2 - u_{j-1}^2\big) = (1-e^{-\mu h})\sum_{j=1}^{J} w_j u_j^2 + e^{-\mu h} w_J u_J^2 - w_1 u_0^2$ (using $w_j - w_{j+1} = (1-e^{-\mu h})w_j$, $w_1 = e^{-\mu h}$, $w_J = e^{-\mu}$). □

Lemma 5. *Every solution of the scheme satisfies ($\sigma h = \tau$) $(1+\tau\nu_h)V^{n+1} + \mathcal{B}^{n+1} \le V^n - 2\tau a^n Q^n + \tau^2 (a^n)^2 M_h$,* (21) *where $Q^n = h\sum_{j=1}^{J} p\, e^{-\mu x_j} R_j^n + h\sum_{j=0}^{J-1} q\, e^{\mu x_j} S_j^n$ and $\mathcal{B}^{n+1} = \tau e^{-\mu h}\Big[p\Big(e^{-\mu}\big(R_J^{n+1}\big)^2 - (R_0^{n+1})^2\Big) + q\Big((S_0^{n+1})^2 - e^{\mu}\big(S_J^{n+1}\big)^2\Big)\Big]$.*

Proof. For the R family we apply Lemma 4 with $u_j = R_j^{n+1}$, $f_j = R_j^n - \tau a^n$, multiply by p and drop the dissipative term; here $h\sum p w_j f_j^2 = V_R^n - 2\tau a^n h\sum p w_j R_j^n + \tau^2 (a^n)^2 h\sum p w_j$. For the S family, the change of index $i = J - j$ brings (14) to the form (13); then $q e^{\mu x_j} = q e^{\mu} e^{-\mu x_i}$, the inflow node is S_J and the outflow node is S_0. Lemma 4 yields the boundary term $\tau e^{-\mu h} q\,\big(S_0^2 - e^{\mu} S_J^2\big)$. Adding the two results completes the proof. □

Lemma 6. $Q^n = 2pP^n + \mathcal{E}^n$, *where $(\mathcal{E}^n)^2 \le \Gamma_h V^n$; moreover, $(P^n)^2 \le \frac{1}{4} Z_h V^n$ and $(\mathcal{H}^n)^2 \le \frac{1}{4} Z_h V^n$.*

Proof. $\mathcal{E}^n = h\sum_{j\ge1} p\,(e^{-\mu x_j}-1)R_j^n + h\sum_{j\le J-1}(qe^{\mu x_j}-p)\,S_j^n$; writing each term as $\frac{c_j}{\sqrt{\omega_j}}\cdot\sqrt{\omega_j}\,u_j$ (where ω_j is the weight in (18)), we apply the discrete Cauchy–Schwarz inequality. The same argument with $c_j = \pm\frac{1}{2}$ applies to P^n and $\mathcal{H}^n$. □

Theorem 1 (Exponential stability of the discrete scheme). *Let* $k \ge 0$, $|r|<1$, $\eta \ge 0$, $h = 1/J$, $\tau > 0$, *and suppose there exist* $\mu > 0$, $q \ge p > 0$, $\theta \in (0,1)$ *such that* (i) $\frac{q}{p}\,r^2e^{2\mu} < 1$, (ii) $\tau k M_h \le 4p(1-\theta)$, (iii) $\nu_h > \theta_h := \frac{k\,\Gamma_h}{4p\theta} + \vartheta_h$. (22) *Then every solution of the scheme satisfies*

$$(1+\tau\nu_h)V^{n+1} \le (1+\tau\theta_h)V^n - \tau k D_h (P^n)^2, \qquad D_h = 4p(1-\theta) - \tau k M_h \ge 0, \qquad (23)$$

and, consequently,

$$V^{n+1} \le q_* V^n, \quad q_* = \frac{1+\tau\theta_h}{1+\tau\nu_h} < 1, \qquad \| u^n \| \le \sqrt{q/p\; e^{\mu(2-h)}}\; q_*^{n/2}\; \| u^0 \|. \qquad (24)$$

Proof. 1. Boundary term. From $R_0 = -S_0$ we have $p(-R_0^2) + qS_0^2 = (q-p)S_0^2 \ge 0$. At $x = 1$, $S_J = -rR_J + \eta\mathcal{H}^n$; we apply Young's inequality $S_J^2 \le (1+\varepsilon)r^2R_J^2 + (1+\varepsilon^{-1})\eta^2(\mathcal{H}^n)^2$ with $(1+\varepsilon) = \frac{p\,e^{-2\mu}}{q\,r^2}$ ($\varepsilon > 0$ by (i); for $r = 0$ the estimate is immediate). Then $1+\varepsilon^{-1} = \left(1 - \frac{q}{p}r^2e^{2\mu}\right)^{-1}$ and

$$pe^{-\mu}R_J^2 - qe^{\mu}S_J^2 \ge -\frac{qe^{\mu}\eta^2}{1-\frac{q}{p}r^2e^{2\mu}}(\mathcal{H}^n)^2.$$

By Lemma 6, $(\mathcal{H}^n)^2 \le \frac{1}{4}Z_hV^n$; therefore $\mathcal{B}^{n+1} \ge -\tau\vartheta_hV^n$.

2. Nonlocal source. From $a^n = kP^n$ and $Q^n = 2pP^n + \mathcal{E}^n$,

$$-2\tau a^nQ^n + \tau^2(a^n)^2M_h = -\tau k(P^n)^2(4p - \tau k M_h) - 2\tau k P^n\mathcal{E}^n.$$

By $2|P\mathcal{E}| \le 4p\theta P^2 + \mathcal{E}^2/(4p\theta)$ and $(\mathcal{E}^n)^2 \le \Gamma_hV^n$, this expression is $\le -\tau k D_h(P^n)^2 + \tau\frac{k\Gamma_h}{4p\theta}V^n$; by (ii), $D_h \ge 0$.

3. Combination. Substituting steps 1–2 into (21) yields (23). By (iii), $\theta_h < \nu_h$ and $q_* < 1$; the norm estimate follows from (19): $\| u^n \|^2 \le \frac{V^n}{pe^{-\mu}} \le \frac{q_*^nV^0}{pe^{-\mu}} \le \frac{qe^{\mu(1-h)}}{pe^{-\mu}}q_*^n\,\| u^0 \|^2$. □

Remark 1 (Meaning of the conditions). (a) The theorem does not require the CFL condition: condition (ii) stems from the explicit treatment of the nonlocal source and is a mild, h-independent restriction $\tau \le 4p(1-\theta)/(kM_h)$ ($M_h \approx p+q$); for $k = 0$ it is absent. (b) As $h \to 0$, $\nu_h \to \mu$, $\Gamma_h \to \Gamma = p\int_0^1(1-e^{-\mu x})^2\,e^{\mu x}\,\mathrm{d}x + \int_0^1(qe^{\mu x}-p)^2\,e^{-\mu x}q^{-1}\,\mathrm{d}x$, and (iii) passes to the continuous condition. (c) *In the passive case* ($k = 0$, $\eta = 0$) the conditions reduce to $q = p$ and $\mu < \ln(1/|r|)$; as $\tau \to 0$, $\mu \to \ln(1/|r|)$, the rate for V is $\ln(1/|r|)$, i.e. $\frac{1}{2}\ln(1/|r|)$ for the amplitude, which is the exact spectral abscissa of the continuous problem (Section 5). Hence in this case the estimate cannot be improved (it

is sharp). (d) The terms with $k > 0$ and $\eta > 0$ increase θ_h: the theorem provides a quantitative guarantee that they *do not destroy stability*; the benefit of the feedback manifests itself in the fundamental mode (Proposition 4).

Corollary 1 (Momentum dissipation and velocity budget). *Under the conditions of Theorem 1, if* $k > 0$ *and* $D_h > 0$, *then* $\sum_{n=0}^{N} \tau\,(P^n)^2 \le \frac{(1+\tau\nu_h)V^0}{kD_h} \quad \forall N,$ (25) *the velocity change of the vehicle* $\Delta v^N = \sum_{n<N} \tau\, a^n$ *converges as* $N \to \infty$, *and* $|\Delta v^\infty| \le \frac{k\tau}{2}\frac{\sqrt{Z_h V^0}}{1-\sqrt{q_*}}.$ (26)

Proof. Since $\theta_h < \nu_h$, (23) gives $(1+\tau\nu_h)V^{n+1} \le (1+\tau\nu_h)V^n - \tau k D_h (P^n)^2$; the telescoping sum yields (25). By Lemma 6 and (24), $|P^n| \le \frac{1}{2}\sqrt{Z_h V^0}\, q_*^{n/2}$, and the geometric series converges. □

4.1. Stability of the B-Variant

Lemma 7 (Discrete momentum balance). *For one step of the A-variant (the predictor),* $\tilde{P}^{n+1} - P^n = -\tau\big(\tilde{F}^{n+1} + a^n\big), \qquad \tilde{F}^{n+1} = \tilde{h}_J - \tilde{h}_0 = 1/2\left((1+r)\tilde{R}_J - \eta\mathcal{H}^n\right) + \tilde{S}_0,$ (27) *which is the exact discrete analogue of the balance* $\dot{P} = -\big(h(t,1) - h(t,0)\big) - a$ *implied by (2). If* $\tilde{V}^{n+1} \le V^n$, *then*

$$\left|\tilde{P}^{n+1} - P^n\right| \le \tau\,\Psi_h\sqrt{V^n}, \qquad \Psi_h = \left(\frac{(1+|r|)e^{\mu/2}}{2\sqrt{p}} + \frac{1}{\sqrt{q}}\right)h^{-1/2} + \left(\frac{\eta}{4} + \frac{k}{2}\right)\sqrt{Z_h}. \quad (28)$$

Proof. Multiplying (13) by h and summing over $j = 1, \dots, J$ (a telescoping sum, $hJ = 1$), we get $h\sum\big(\tilde{R}_j - R_j\big) = -\tau\big(\tilde{R}_J - \tilde{R}_0\big) - \tau a^n$; similarly, (14) gives $h\sum\big(\tilde{S}_j - S_j\big) = \tau\big(\tilde{S}_J - \tilde{S}_0\big) - \tau a^n$. We add half of each, and use $\tilde{h} = \frac{1}{2}\big(\tilde{R} - \tilde{S}\big)$ and the boundary conditions. For the estimate: $hpe^{-\mu}\tilde{R}_J^2 \le \tilde{V}^{n+1}$, $hq\tilde{S}_0^2 \le \tilde{V}^{n+1}$, and, by Lemma 6, $|\mathcal{H}^n|, |P^n| \le \frac{1}{2}\sqrt{Z_h V^n}$. □

Theorem 2 (Exponential stability of the B-variant). *Let the conditions of Theorem 1 hold with* (μ, q, θ), *let* $c_h := 4p - \tau k M_h > 0$, *and let* $\nu_h > \theta_h^{\mathrm{B}} := \vartheta_h + \frac{k\left(\sqrt{\Gamma_h} + p\,\tau\,\Psi_h\right)^2}{\theta\, c_h}.$ (29) *Then the solution of the B-variant satisfies* $(1+\tau\nu_h)V^{n+1} \le \big(1+\tau\theta_h^{\mathrm{B}}\big)V^n - \tau k(1-\theta)c_h\left(P^{n+1/2}\right)^2;$ (30) *hence* $V^{n+1} \le q_{\mathrm{B}} V^n$, $q_{\mathrm{B}} = \big(1+\tau\theta_h^{\mathrm{B}}\big)/(1+\tau\nu_h) < 1$, *and* $\| u^n \| \le \sqrt{\frac{q}{p}e^{\mu(2-h)}}\, q_{\mathrm{B}}^{n/2} \| u^0 \|$.

Proof. 0. Predictor. The predictor is one step of the A-variant; hence, by Theorem 1, $\tilde{V}^{n+1} \le q_* V^n \le V^n$, and Lemma 7 applies.

1. Boundary term. In the corrector, Lemma 5 holds with $a^{n+1/2}$ and $\mathcal{H}^{n+1/2}$. Since $\left(\mathcal{H}^{n+1/2}\right)^2 \le \frac{1}{2}\left((\mathcal{H}^n)^2 + \left(\widetilde{\mathcal{H}}^{n+1}\right)^2\right) \le \frac{Z_h}{8}\left(V^n + \tilde{V}^{n+1}\right) \le \frac{Z_h}{4}V^n$, step 1 of the proof of Theorem 1 repeats without change and gives $\mathcal{B}^{n+1} \ge -\tau\vartheta_h V^n$.

2. Nonlocal source. $Q^n = 2pP^n + \mathcal{E}^n = 2pP^{n+1/2} + p\left(P^n - \tilde{P}^{n+1}\right) + \mathcal{E}^n$. Hence

$$-2\tau a^{n+1/2}Q^n + \tau^2\left(a^{n+1/2}\right)^2 M_h = -\tau k\, c_h \left(P^{n+1/2}\right)^2 - 2\tau k P^{n+1/2}\left(p\left(P^n - \tilde{P}^{n+1}\right) + \mathcal{E}^n\right).$$

By (28) and Lemma 6, $\left|p\left(P^n - \tilde{P}^{n+1}\right) + \mathcal{E}^n\right| \le \left(p\tau\Psi_h + \sqrt{\Gamma_h}\right)\sqrt{V^n}$. With Young's inequality $2|x|y \le \theta c_h x^2 + y^2/(\theta c_h)$ this expression is $\le -\tau k(1-\theta)c_h\left(P^{n+1/2}\right)^2 + \tau\frac{k\left(\sqrt{\Gamma_h}+p\tau\Psi_h\right)^2}{\theta c_h}V^n$.

3. Substituting steps 1–2 into (21) yields (30); the rest is as in the proof of Theorem 1. □

Remark 2. (a) For fixed $\sigma = \tau/h$ and $h \to 0$, $p\tau\Psi_h = O\left(\sigma\sqrt{h} + \tau\right) \to 0$, i.e. $\theta_h^{\mathrm{B}} \to \vartheta_h + k\Gamma_h/(4p\theta)$, the same as the estimate for the A-variant; for small steps the certificate of the B-variant differs little from that of the A-variant. (b) Theorem 2 requires the conditions of Theorem 1, in particular (ii), for the predictor; numerical experiments (Section 6.9) show that the B-variant remains stable far beyond this condition; proving stability in this region is an open problem.

5. SPECTRAL ANALYSIS AND THE FUNDAMENTAL MODE

Solutions of the continuous linearized problem of the form e^{st} are $R = Ae^{-sx} - a_0/s$, $S = Be^{sx} - a_0/s$, with $a_0 = kP_0$. The boundary conditions and (7) give a homogeneous system for (A, B, a_0):

$$\det\begin{pmatrix} 1 & 1 & -2/s \\ re^{-s} - \frac{\eta}{2}E_1 & e^{s} + \frac{\eta}{2}E_2 & -(1+r)/s \\ -\frac{k}{2}E_1 & -\frac{k}{2}E_2 & 1 + k/s \end{pmatrix} = 0, \qquad E_1 = \frac{1-e^{-s}}{s},\ E_2 = \frac{e^{s}-1}{s}. \qquad (31)$$

For $k = \eta = 0$ all roots are $s = -\delta + in\pi$, $\delta = \frac{1}{2}\ln(1/r)$ $(0 < r < 1)$: all modes decay at the same rate.

Proposition 4 (First-order formula for the fundamental mode). *Let k and δ be small and $\eta = 0$. Then the decay rate of the nth mode is* $-\mathrm{Re}s_n = \delta + \frac{4k}{n^2\pi^2}\frac{1-(-1)^n}{2} + O(k^2 + \delta^2 + k\delta)$, (32) *i.e. the feedback damps only the odd modes (those with nonzero sloshing force $F_s \neq 0$), and its strongest effect is on the fundamental mode ($n = 1$).*

Heuristic argument. For the mode $h = \cos(n\pi x)\cos(n\pi t)$, $v = \sin(n\pi x)\sin(n\pi t)$ at $k = 0$, $r = 1$, we have $E = \frac{1}{4}$ and $P = \frac{1-(-1)^n}{n\pi}\sin(n\pi t)$. By (8), the period-averaged dissipation is $k\langle P^2\rangle = \frac{2k}{n^2\pi^2}\cdot\frac{1-(-1)^n}{2}$; the amplitude decay rate equals $\langle\text{dissipation}\rangle/(2E)$. The wall dissipation gives δ in the same way. The formula is verified against the exact roots of (31) in Section 6.3. □

Two practical conclusions follow from (32): (a) for a required damping ratio ζ_* of the fundamental mode, $k \approx \frac{\pi^2}{4}(\pi\zeta_* - \delta)$; (b) for $k < 0$ the fundamental mode loses stability when $k < k_{\mathrm{cr}} \approx -\pi^2\delta/4$.

6. NUMERICAL EXPERIMENTS

6.1. Parameters

Dimensional example: $L = 2$ m, $H_0 = 0.2$ m, $g_e = 0.5$ m/s^2; then $c = 0.316$ m/s, the time unit is $L/c = 6.32$ s, and the fundamental-mode period is $2L/c = 12.6$ s. In the baseline case $r = 0.9$ ($\zeta_d = 19$), which corresponds to a passive damping of the fundamental mode of $\zeta_1 = 1.7\%$ (a typical value for baffled tanks). The initial state is the tilted surface after a constant-acceleration manoeuvre: $h(0,x) = -A\left(x - \frac{1}{2}\right)$, $v(0,x) = 0$ ($\int h = 0$). To ensure that the scheme error does not distort the sloshing physics, the main computations were carried out with $J = 4000$, $\tau = h$ ($\sigma = 1$); comparisons with the Lyapunov estimate used $J = 1000$, $\tau = h$; and the spectral analysis used $J = 400$, $\tau = h$.

6.2. Decay of Sloshing

Figure 1 shows the space–time plot of the free-surface elevation $h(t,x)$: for $k = 0$ the fundamental mode oscillates for a long time, while for $k = 2$ it decays within $t \approx 3$. Figure 2 shows the sloshing force F_s and the velocity change Δv of the vehicle; the numerical values are given in Table 1. For $k = 2$ the maximal force for $t > 10$ is reduced 18-fold, and for $t > 20$ 50-fold; the velocity budget spent on this is $\Delta v = 0.0166\,c \approx 5.2$ mm/s (for $A = 0.1$).

Insert Figure 1

Insert Figure 2

Insert Table 1

6.3. Lyapunov Estimate and Decay Rates

Figure 3 shows $\| u^n \|$, V^n and the bound of Theorem 1 (dotted lines); in all cases the inequality $V^{n+1} \leq q_* V^n$ was verified numerically at every step. In Table 2: $\alpha_L = -\ln q_* / (2\tau)$ is the rate guaranteed by the theorem; α_S is the rate given by the spectral radius of the iteration matrix of the scheme; α_C is the spectral abscissa of the continuous problem computed from the exact roots of (31); ζ_1 is the damping ratio of the fundamental mode ($-\mathrm{Re} s_1 / |s_1|$). For $\eta = 0$, $\alpha_L \leq \alpha_S \approx \alpha_C$, and in the passive case $\alpha_L = \alpha_C$ (Remark 1(c)). For $\eta = 0.3$ the estimate is conservative, while the excess $\alpha_S > \alpha_C$ is due to numerical dissipation of high-frequency modes ($O(h)$, vanishing as $h \to 0$). The most important column is ζ_1: the feedback raises it from 1.7% ($k = 0$) to 14.5%, 27%, 52% ($k = 1,2,4$); for $r = 0.98$ (an almost rigid wall) from 0.32% to 26%. The overall abscissa α_C, by contrast, hardly changes: it is determined by the even modes and the zero-frequency mode, which the feedback cannot influence (Proposition 1).

Insert Figure 3

Insert Table 2

6.4. Stability Map and Choice of k

Figure 4 (left): the spectral decay rate of the scheme in the (k, r) plane, its zero level set, and the region guaranteed by Theorem 1 (hatched, $k \geq 0$). The stability boundary is $k_{\mathrm{cr}}(r) < 0$: from (31), $k_{\mathrm{cr}} = -0.621$ ($r = 0.6$), -0.1299 ($r = 0.9$), -0.0249 ($r = 0.98$), in agreement with the values $-\pi^2 \delta / 4 = -0.630,\ -0.1300,\ -0.0249$ obtained from (32). Right: $\zeta_1(k)$; for $r = 0.9$, (32) predicts that $k \approx 0.645$ is needed for $\zeta_* = 10\%$, while the exact roots give the interval $k \in (0.5;\ 0.75)$ ($\zeta_1 =$ 8.1% and 11.3%).

Insert Figure 4

6.5. Unstable and Non-Decaying Regimes

Figure 5 (left): for $k < 0$ (the tank is accelerated against the motion of the liquid) the disturbance grows exponentially; by (31), the growth rates are 0.150, 0.353, 0.763 ($k = -0.5, -1, -2$, $r = 0.9$), with a frequency close to that of the fundamental mode. Right: rigid walls ($r = 1$) and $k = 2$, even mode $h = 0.05\cos(2\pi x)$. In the continuous problem it does not decay (Proposition 1); the decay rates observed for the scheme are 0.295, 0.074, 0.0185 ($J = 200{,}800{,}3200$, $\tau = 2h$), i.e. they decrease fourfold each time h is reduced fourfold, so the decay is purely numerical dissipation.

Insert Figure 5

6.6. CFL Condition

Figure 6: in a physically stable regime ($k = 2$, $r = 0.9$) the explicit scheme blows up for $\sigma = 1.05$, whereas the IMEX scheme is stable for $\sigma = 1.05$ and $\sigma = 4$.

Insert Figure 6

6.7. Nonlinear Model

Figure 7 shows results for large-amplitude sloshing ($A = 0.3$) computed with the fully nonlinear form of (1) in Riemann invariants ($R = V + 2\sqrt{H}$, $S = V - 2\sqrt{H}$, with the speeds $\lambda_{\pm} = V \pm \sqrt{H}$ frozen at each node, $a = k\int_0^1 H\,V\,\mathrm{d}x$): steep fronts (waves close to hydraulic jumps) form on the surface. The force for $t > 10$ is $0.217A$ for $k = 0$ and $0.0102A$ for $k = 2$ (21 times smaller). At small amplitude ($A = 0.001$) the nonlinear computation agrees with the linear scheme. No proof for the nonlinear case is given in this paper: a scheme of this type in Riemann invariants does not compute shock waves conservatively, so these results are to be interpreted qualitatively.

Insert Figure 7

6.8. Order of Convergence

Table 3: errors at $T = 1$ relative to the solution with $J = 12800$ for smooth compatible initial data; the observed order satisfies $p_{\mathrm{obs}} \to 1$.

Insert Table 3

6.9. Comparison of the A- and B-Variants

(a) *Stability certificate.* The conditions of Theorem 2 were also verified numerically at every step (random initial data, 4 different parameter sets, no violations). The guaranteed rate ($k = 2, r = 0.9$) is 0.0507 for A and 0.0381 for B at $J = 200$, $\tau = 0.005$, and 0.0507 and 0.0467, respectively, at $J = 1000$, $\tau = 0.001$; in agreement with Remark 2(a), the difference vanishes as the grid is refined.

(b) *Nonlocal lag error.* The purpose of the B-variant is to reduce the error caused by lagging the nonlocal terms by one time level. To measure this error separately, we compared both variants on the same grid with a *fully implicitly coupled* scheme (I-variant: $a^{n+1} = kP^{n+1}$, $\mathcal{H}^{n+1}$ at the new level, a 2×2 linear system at each step) (Table 4): the lag error of the B-variant is ≈ 2 times smaller than that of the A-variant for all σ (B has a half-level lag, A a full-level lag), while the order remains first, since the transport operator is first-order (implicit Euler).

(c) *Overall accuracy.* With respect to the solution of the partial differential equation (PDE) problem (reference $J = 8000$) there is practically no difference in error (Table 5): the overall error is governed by the first-order dissipation of the transport operator, and the nonlocal lag is smaller than it. The velocity budget Δv at $J = 400$ also differs from the reference value (0.01635) by less than 0.1% for both variants.

(d) *Stability for large time steps* is the main advantage of the B-variant. Figure 8: for $k = 8$, $\tau = 0.5$ the A-variant grows exponentially, whereas the B-variant decays. Spectral analysis at $J = 60$: the A-variant is unstable for $\tau \in [0.45; 1.0]$ at $k = 8$ and for $\tau \geq 0.15$ at $k = 16$; the B-variant is stable for all tested $\tau \leq 3$ at $k = 8$, and at $k = 16$ it is unstable only for $\tau \in [0.25; 0.55]$. The reason is that under strong feedback ($k\tau = O(1)$) the one-step lag of the nonlocal source itself becomes a source of instability; the half-level corrector reduces it substantially.

Insert Table 4

Insert Table 5

Insert Figure 8

---

7. APPLICATION TO A REAL TANK: P/N 80451-1 (WORLDVIEW-4)

The P/N 80451-1 hydrazine diaphragm tank manufactured by Northrop Grumman was used on the GeoEye-2 (WorldView-4) spacecraft [17]: volume 623 L, inner diameter 1021 mm, length 1011 mm (oblate spheroid), empty mass 49.9 kg, up to 454 kg of hydrazine, with an internal baffle dome. We approximate the tank by a sphere of equivalent radius 0.509 m; the hydrazine density is $\rho \approx 1004$ kg/m^3 and the surface tension ≈ 0.066 N/m. In the equivalent 1D model, L is the width W of the free surface of the settled liquid and H_0 is the mean depth (volume divided by free-surface area). As an example, the effective acceleration is taken to be $g_e = 0.05$ m/s^2 (the time scale is proportional to $g_e^{-1/2}$). The general view of the tank, its cross-section with the notation of the equivalent model, and the liquid motion inside the tank are shown in Figure 9. Panels (c)–(d) of the figure present the results of the linear model of this paper and the A-variant ($J = 400$, $\tau = h$) for the tank at 30% fill, placed onto the tank cross-section in dimensional units ($\eta = H_e h$, $t = (L/c_e)\, t'$); the shape of the fundamental sloshing mode in spherical tanks and the tilted free surface after a manoeuvre agree with the descriptions in [1, 3]. For $k = 0$ the fundamental-mode period is $T_1 \approx 19.7$ s, so at $t = 20$ and 40 s the surface returns almost to its initial tilted state (the damping is only $\zeta_1 = 1.7\%$), whereas for $k = 2$ the surface is almost flat by this time and the flow velocities in the tank (arrows) are considerably smaller. The results are given in Table 6; the decay times and Δv were recalculated from the dimensionless results of Tables 1 and 2 ($r = 0.9$) via L/c_e and c_e.

Insert Figure 9

Insert Table 6

Conclusions. (1) For the full tank the shallow-water model underestimates the fundamental period by 37% (9.5 instead of 15.1 s); the equivalent model removes this error and gives the correct

sloshing mass (32%). (2) The Bond number is $\gg 1$, i.e. with the engine firing the liquid is indeed "settled" and the gravity-dominated sloshing model is applicable. (3) Feedback with $k = 2$ shortens the decay time of the fundamental mode from ≈ 150–210 s to ≈ 9–13 s, at the cost of a few mm/s of velocity. (4) In the real tank the elastomeric diaphragm covers the whole surface and may restrain sloshing more strongly than in the model; in the model it is represented by an equivalent passive damper r, and r has to be calibrated for the specific tank by experiment or computational fluid dynamics (CFD). Since the spherical geometry is replaced by a rectangular equivalent, the values in Table 6 are engineering estimates.

8. PRACTICAL RECOMMENDATIONS

1. The feedback works only in combination with passive dissipation ($|r| < 1$: diaphragm, baffles) (Proposition 1); the even modes produce no force, but they too are damped only passively.
2. The sign of the gain matters: $k < 0$ destabilizes the fundamental mode for $k < k_{\text{cr}} \approx -\pi^2\delta/4$; hence a sign error in measurement or modelling is dangerous.
3. k can be chosen from (32): $\zeta_* \approx (\delta + 4k/\pi^2)/\pi$; $k \approx 2$ damps the fundamental mode to $\approx 27\%$ and reduces the sloshing force 18–50-fold, with a small velocity budget (≈ 5 mm/s for $A = 0.1$).
4. Under strong feedback ($k\tau \gtrsim 1$, e.g. $k \geq 8$) or for large time steps the B-variant should be used: it costs twice as much, but it is stable in the region where the A-variant is unstable. For small $k\tau$ the A-variant is sufficient.
5. For on-board computations the IMEX scheme is recommended: it is stable without the CFL condition, one step requires $O(J)$ operations, and its stability is guaranteed by Theorem 1. The numerical dissipation of the first-order scheme over-damps a mode of frequency ω by approximately $\frac{h}{2}(1+\sigma)\omega^2$; to capture the physical damping δ correctly, one needs $h(1+\sigma)\omega^2 \ll 2\delta$.

9. CONCLUSIONS

For propellant sloshing in a spacecraft tank, a linearized problem based on the Saint-Venant model with two nonlocal mechanisms, a nonlocal boundary condition resulting from volume conservation and nonlocal momentum feedback, has been formulated. For this problem a new two-sided upwind implicit–explicit scheme has been constructed, the boundary-closure formula has been

proved, and, by means of a classical discrete Lyapunov function with exponential weights, the exponential stability of the scheme without the CFL condition has been proved under conditions depending explicitly on the grid parameters; in the passive case the estimate is sharp. A predictor–corrector B-variant for the nonlocal terms has also been constructed and its stability proved; it halves the nonlocal lag error and is more stable for large time steps under strong feedback. Estimates for the momentum dissipation and the velocity budget have been obtained, and it has been shown that stabilization is impossible without passive damping and that the system is unstable for $k < 0$. Spectral analysis and numerical experiments have confirmed that the feedback effectively damps the fundamental sloshing mode. The model has been extended to deep tanks by means of an equivalent depth and applied to the 623 L hydrazine tank of the WorldView-4 spacecraft. Future work will address discrete C^1-estimates for the nonlinear model, a model coupled with rotational (pitch) motion, and networked (multi-tank) systems.

Compliance with Ethical Standards

Funding: This research received no external funding; it was carried out at the authors' own expense.

Conflicts of Interest: The authors declare that they have no conflict of interest.

REFERENCES

1. Abramson HN (ed) (1966) The dynamic behavior of liquids in moving containers. NASA SP-106. National Aeronautics and Space Administration, Washington, DC
2. Dodge FT (2000) The new “Dynamic behavior of liquids in moving containers”. Southwest Research Institute, San Antonio, TX
3. Ibrahim RA (2005) Liquid sloshing dynamics: theory and applications. Cambridge University Press, Cambridge
4. Dubois F, Petit N, Rouchon P (1999) Motion planning and nonlinear simulations for a tank containing a fluid. In: Proceedings of the European Control Conference, Karlsruhe
5. Petit N, Rouchon P (2002) Dynamics and solutions to some control problems for water-tank systems. IEEE Trans Automat Control 47:594-609
6. Coron JM (2002) Local controllability of a 1-D tank containing a fluid modeled by the shallow water equations. ESAIM Control Optim Calc Var 8:513-554
7. Coron JM, Hayat A, Xiang S, Zhang C (2022) Stabilization of the linearized water tank system. Arch Ration Mech Anal. doi:10.1007/s00205-022-01778-0
8. Coron JM, Bastin G, d’Andréa-Novel B (2008) Dissipative boundary conditions for one-dimensional nonlinear hyperbolic systems. SIAM J Control Optim 47:1460-1498
9. Bastin G, Coron JM, d’Andréa-Novel B (2009) On Lyapunov stability of linearised Saint-Venant equations for a sloping channel. Netw Heterog Media 4:177-187
10. Bastin G, Coron JM (2016) Stability and boundary stabilization of 1-D hyperbolic systems. Progress in Nonlinear Differential Equations and Their Applications, vol 88. Birkhäuser, Cham
11. Banda MK, Herty M (2013) Numerical discretization of stabilization problems with boundary controls for systems of hyperbolic conservation laws. Math Control Relat Fields 3:121-142
12. Göttlich S, Schillen P (2017) Numerical discretization of boundary control problems for systems of balance laws: feedback stabilization. Eur J Control 35:11-18
13. Aloev RD, Khudayberganov MU (2018) A discrete analogue of the Lyapunov function for hyperbolic systems. Sovrem Mat Fundam Napravl 64:591-602

14. Aloev RD, Berdyshev AS, Alimova V, Bekenayeva KS (2024) Exponential stability of the numerical solution of a hyperbolic system with nonlocal characteristic velocities. Axioms 13:334

15. Aloev R, Berdyshev A, Alimova V (2025) Exponential stability of a numerical solution of a hyperbolic system with negative nonlocal characteristic velocities and measurement error. Uzbek Math J 69:7-14

16. Berdyshev A, Aloev R, Abdiramanov Zh, Ovlayeva M (2023) An explicit–implicit upwind difference splitting scheme in directions for a mixed boundary control problem for a two-dimensional symmetric t-hyperbolic system. Symmetry 15:1863

17. Northrop Grumman. Diaphragm tanks data sheets sorted by volume: P/N 80451-1. https://www.northropgrumman.com/what-we-do/space/mission-enabling-products/diaphragm-tanks-data-sheets-sorted-by-volume. Accessed 20 October 2026

Tables

Table 1. Sloshing force and velocity budget ($r = 0.9$, $\eta = 0$, $A = 0.1$, $J = 4000$, $\tau = h$).

k	$\max_{t>10}\lvert F_s\rvert$	$\max_{t>20}\lvert F_s\rvert$	$\Delta v(40)$
0	5.25e-02	2.93e-02	0.0000
1	4.78e-03	1.13e-03	0.0083
2	2.93e-03	5.86e-04	0.0166
4	1.79e-03	2.26e-04	0.0331

Table 2. Decay rates and damping ratio of the fundamental mode (α_L, α_S: $J = 400$, $\tau = h$; α_C, ζ_1: exact roots of (31)).

k	r	η	μ_{opt}	α_L	α_S	α_C	$-\mathrm{Res}_1$	ζ_1, %
0	0.9	0	0.105	0.0527	0.0527	0.0527	0.0527	1.68
1	0.9	0	0.105	0.0517	0.0520	0.0520	0.4585	14.49
2	0.9	0	0.105	0.0507	0.0513	0.0513	0.8670	27.18
4	0.9	0	0.105	0.0488	0.0500	0.0500	1.7014	52.36
0	0.98	0	0.020	0.0101	0.0101	0.0101	0.0101	0.32
2	0.98	0	0.020	0.0100	0.0101	0.0101	0.8244	26.12
0	0.6	0	0.511	0.2551	0.2552	0.2554	0.2554	8.10
2	0.6	0	0.511	0.2087	0.2251	0.2252	1.0766	32.03
0	0.6	0.3	0.314	0.0607	0.2801	0.2554	0.2557	8.15
1	0.6	0.3	0.301	0.0524	0.3538	0.2554	0.6722	20.74
2	0.6	0.3	0.288	0.0447	0.3538	0.2554	1.0895	32.50

Table 3. Order of convergence ($k = 2$, $r = 0.9$, $\tau = 0.8h$).

J	E_h	p_{obs}
100	1.407e-02	–
200	7.603e-03	0.89
400	3.909e-03	0.96
800	1.934e-03	1.02
1600	9.124e-04	1.08

Table 4. Nonlocal lag error relative to the fully implicitly coupled scheme, $\max_n \| u^n_{\mathrm{A,B}} - u^n_{\mathrm{I}} \|_{\ell_2}$ **(**$k = 2, r = 0.6, \eta = 0.3, J = 400, T = 10$**).**

σ	τ	A-variant	B-variant	ratio
1	0.0025	9.75e-05	4.86e-05	2.01
2	0.0050	1.91e-04	9.47e-05	2.01
4	0.0100	3.67e-04	1.81e-04	2.03
8	0.0200	6.83e-04	3.32e-04	2.06
16	0.0400	1.21e-03	5.71e-04	2.11

Table 5. Maximal error on $t \in [0,10]$ relative to the PDE reference solution: momentum P and sloshing force F_s ($k = 2, r = 0.9, \eta = 0, J = 400$).

σ	e_P (A)	e_P (B)	e_F (A)	e_F (B)
1	4.59e-04	4.76e-04	8.76e-03	8.77e-03
4	8.25e-04	8.48e-04	1.29e-02	1.29e-02
10	1.45e-03	1.51e-03	1.85e-02	1.83e-02

Table 6. Parameters of the equivalent model for the P/N 80451-1 tank ($g_e = 0.05$ m/s^2, $r = 0.9$). T_1^{SV}: shallow-water model; T_1: equivalent model (identical to (9)); t_e: e-folding time of the fundamental-mode amplitude; $K = kc_e/L$: dimensional gain; Δv: for $A = 0.1$.

Fill level	73% (full)	30%	10%
Hydrazine mass m, kg	457	188	63
Free-surface width $L = W$, m	0.900	0.993	0.828
Mean depth H_0, m; H_0/L	0.714; 0.79	0.241; 0.24	0.116; 0.14
Equivalent depth H_e, m	0.283	0.203	0.109
c_e, m/s	0.119	0.101	0.074
T_1^{SV} / T_1, s	9.5 / 15.1	18.1 / 19.7	21.8 / 22.4
Sloshing mass m_1, kg (%)	147 (32%)	128 (68%)	48 (76%)
Bond number $\rho g_e (L/2)^2/\sigma_s$	154	188	130
t_e: $k = 0$ / $k = 2$, s	144 / 8.7	187 / 11.4	213 / 12.9
K ($k = 2$), s^{-1}	0.264	0.203	0.178
Δv ($k = 2$, $A = 0.1$), mm/s	1.97	1.67	1.22

Figure legends

Fig 1 Free-surface elevation $h(t,x)$ ($r = 0.9$, $\eta = 0$, $A = 0.1$, $J = 4000$): passive damper (left) and momentum feedback with $k = 2$ (right).

Fig 2 Sloshing force $F_s(t)$ (left) and total velocity change of the vehicle $\Delta v(t)$ (right), $r = 0.9$.

Fig 3 ℓ_2-norm (left) and discrete Lyapunov function (right), $J = 1000$, $\tau = h$; dotted lines are the bound (24) of Theorem 1.

Fig 4 Left: stability map in the (k, r) plane ($\eta = 0$, $J = 40$, $\tau = 0.5h$); blue: stable, red: unstable, hatched: guaranteed by Theorem 1. Right: damping ratio of the fundamental mode $\zeta_1(k)$ (exact roots of (31)).

Fig 5 Left: instability for $k < 0$ ($r = 0.9$, $J = 1000$). Right: decay of an even mode in a rigid-walled tank caused solely by numerical dissipation.

Fig 6 Numerical instability of the explicit scheme when the CFL condition is violated, and unconditional stability of the IMEX scheme ($J = 200$).

Fig 7 Nonlinear Saint-Venant model ($r = 0.9$, $J = 2000$): sloshing force (left) and surface profiles for $k = 0$ (right).

Fig 8 A- and B-variants at large time steps. Left: $k = 8$, $\tau = 0.5$, $J = 200$, $r = 0.9$. Right: stability boundaries in the (k, τ) plane ($J = 40$); red: A-variant unstable, blue: B-variant unstable as well.

Fig 9 The P/N 80451-1 tank (WorldView-4) and propellant sloshing in it. (a) Schematic view of the tank (oblate spheroid, Ø 1021 mm × 1011 mm, dimensions from the data sheet [17]; the internal diaphragm and baffle dome are not shown) with hydrazine "settled" by engine thrust at 30% fill. (b) Cross-section, domain $[0, L]$ of the equivalent 1D model, depths H, H_0, H_e and boundary conditions. (c)–(d) Free-surface profiles given by the model of this paper and the velocity field at $t = 5$ s (arrows, same scale in both panels): $k = 0$ and $k = 2$.

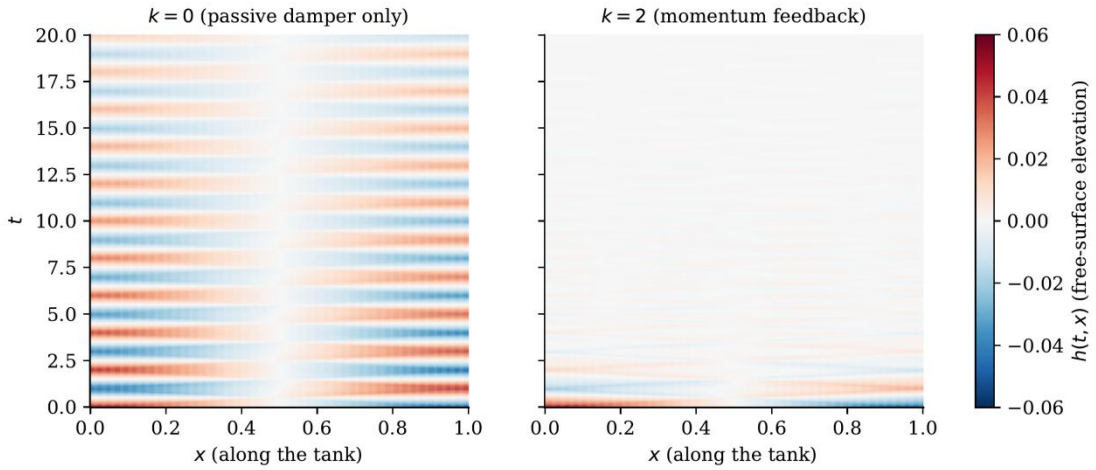
$k = 0$ (passive damper only)
$k = 2$ (momentum feedback)
t
x (along the tank)
x (along the tank)
$h(t, x)$ (free-surface elevation)
0.0
2.5
5.0
7.5
10.0
12.5
15.0
17.5
20.0
0.0
0.2
0.4
0.6
0.8
1.0
0.06
0.04
0.02
0.00
−0.02
−0.04
−0.06

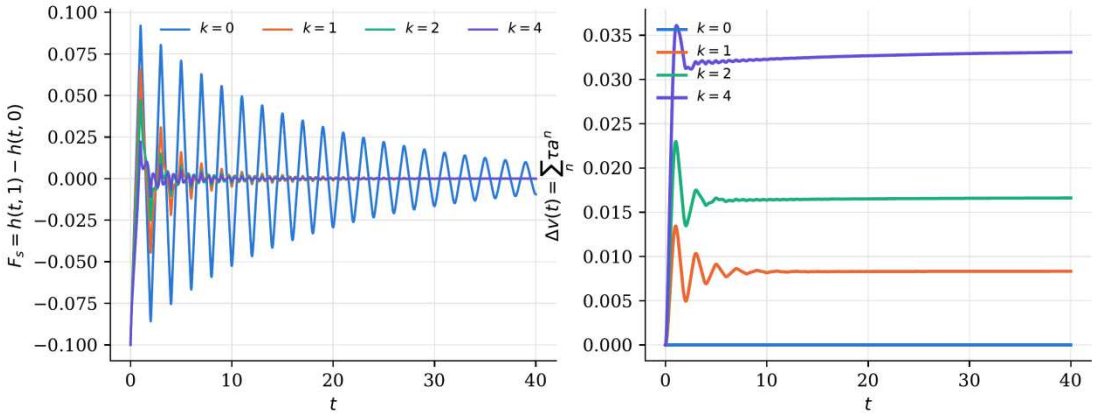
$F_s = h(t,1) - h(t,0)$
$k=0$
$k=1$
$k=2$
$k=4$
t
$\Delta v(t) = \sum_n \tau a^n$
$k=0$
$k=1$
$k=2$
$k=4$
t

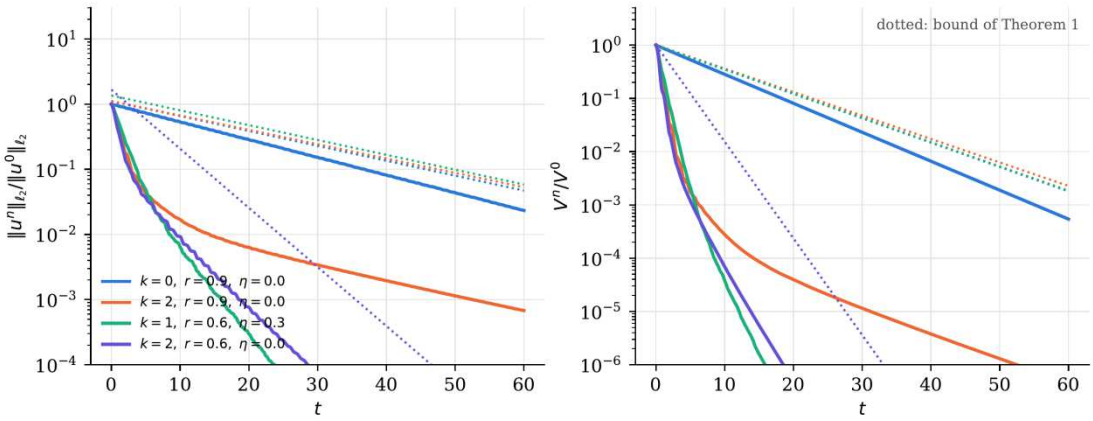
$\|u^n\|_{L_2}/\|u^0\|_{L_2}$
V^n/V^0
t
t
dotted: bound of Theorem 1
$k=0,\ r=0.9,\ \eta=0.0$
$k=2,\ r=0.9,\ \eta=0.0$
$k=1,\ r=0.6,\ \eta=0.3$
$k=2,\ r=0.6,\ \eta=0.0$

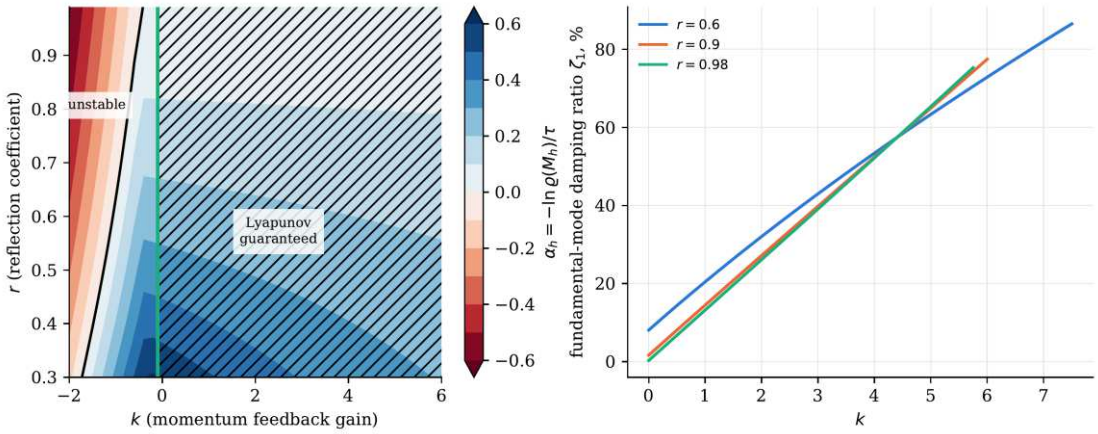
unstable
Lyapunov
guaranteed
r (reflection coefficient)
k (momentum feedback gain)
$\alpha_h = -\ln \varrho(M_h)/\tau$
fundamental-mode damping ratio ζ_1, %
r = 0.6
r = 0.9
r = 0.98
k

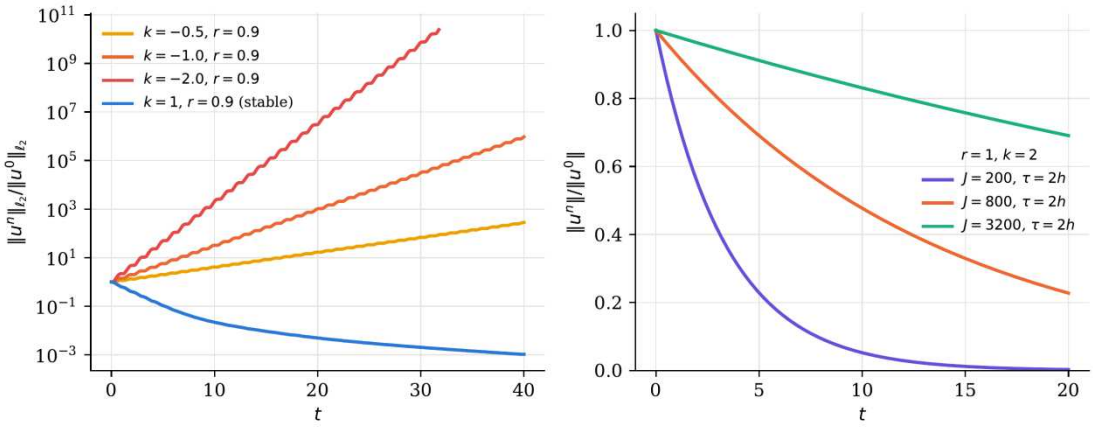
$k = -0.5,\ r = 0.9$
$k = -1.0,\ r = 0.9$
$k = -2.0,\ r = 0.9$
$k = 1,\ r = 0.9$ (stable)
$\|u^n\|_{l_2}/\|u^0\|_{l_2}$
t
$r = 1,\ k = 2$
$J = 200,\ \tau = 2h$
$J = 800,\ \tau = 2h$
$J = 3200,\ \tau = 2h$
$\|u^n\|/\|u^0\|$
t

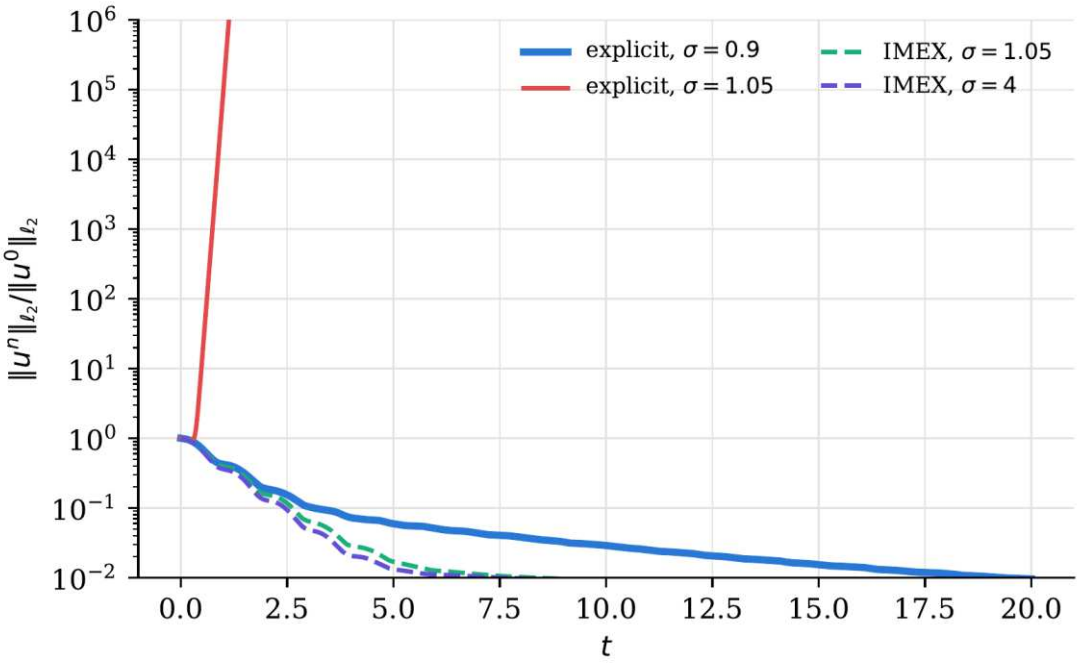
explicit, $\sigma = 0.9$
explicit, $\sigma = 1.05$
IMEX, $\sigma = 1.05$
IMEX, $\sigma = 4$
$\|u^n\|_{\ell_2}/\|u^0\|_{\ell_2}$
10^6
10^5
10^4
10^3
10^2
10^1
10^0
10^{-1}
10^{-2}
0.0
2.5
5.0
7.5
10.0
12.5
15.0
17.5
20.0
t

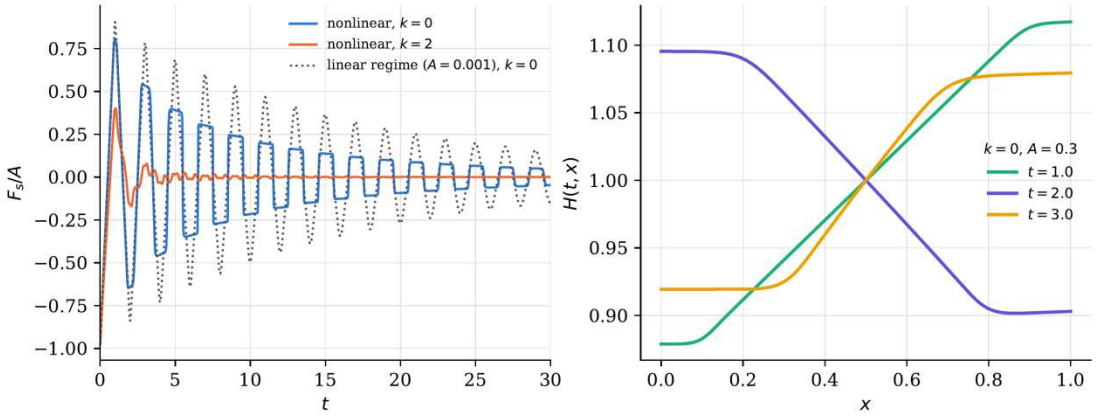
nonlinear, $k = 0$
nonlinear, $k = 2$
linear regime ($A = 0.001$), $k = 0$
F_s/A
t
$H(t, x)$
x
$k = 0$, $A = 0.3$
$t = 1.0$
$t = 2.0$
$t = 3.0$

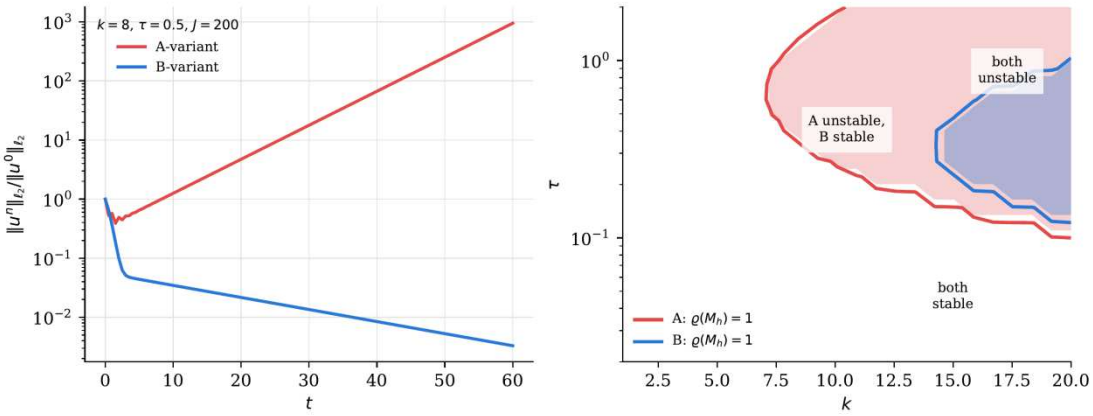
$k = 8,\ \tau = 0.5,\ J = 200$
A-variant
B-variant
$\|u^n\|_{l_2}/\|u^0\|_{l_2}$
t
τ
k
both unstable
A unstable, B stable
both stable
A: $\varrho(M_h) = 1$
B: $\varrho(M_h) = 1$

(a) P/N 80451-1 tank (schematic), 30% fill

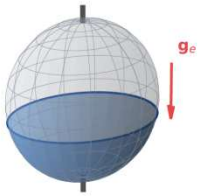

(b) Cross-section and equivalent 1D model notation

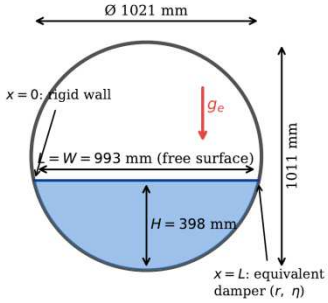

$H_0 = 241$ mm, $H_e = 203$ mm, $c_e = 0.101$ m/s, $T_1 = 19.7$ s

(c) $k = 0$: passive damping only

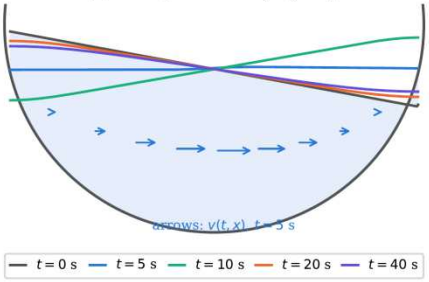

(d) $k = 2$: momentum feedback

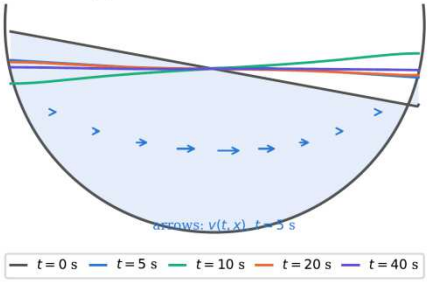

Surface elevation exaggerated 3×; initial tilted-surface amplitude $A = 0.3$ (±30 mm), $r = 0.9$, $g_e = 0.05$ m/s^2.